






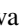



Investigation of isomeric states in ^{255}Rf R. Chakma ^{*}, A. Lopez-Martens , and K. Hauschild *Université Paris-Saclay, CNRS/IN2P3, IJCLab, 91405 Orsay, France*A. V. Yeremin , O. N. Malyshev, A. G. Popeko , Yu. A. Popov, A. I. Svirikhin , V. I. Chepigin, E. A. Sokol ,
A. V. Isaev , A. A. Kuznetsova , M. L. Chelnokov , M. S. Tezekbayeva , and I. N. Izosimov *Flerov Laboratory of Nuclear Reactions, JINR, 141980 Dubna, Russia*O. Dorvaux , B. Gall , and Z. Asfari*Université de Strasbourg, CNRS, IPHC UMR 7178, 67000 Strasbourg, France*

(Received 28 September 2022; accepted 4 January 2023; published 31 January 2023; corrected 13 March 2023)

Using the GABRIELA detector array, γ -ray and internal-conversion-electron decay spectroscopy has been performed on ^{255}Rf nuclei that were produced via the $^{207}\text{Pb}(^{50}\text{Ti}, 2n)^{255}\text{Rf}$ fusion-evaporation reaction using the SHELS velocity filter. Three isomers were identified in ^{255}Rf with the aid of GEANT4 simulations. The existence of two high- K isomeric states in cascade has been confirmed. Possible three-quasiparticle configurations involving the coupling of the unpaired $9/2^- [734]$ neutron to two-quasiparticle states have been suggested and a likely decay scenario has been proposed on the basis of comparisons to GEANT4 simulations. The simulations have also confirmed the existence of the $5/2^+ [622]$ spin isomer at low excitation energy.

DOI: [10.1103/PhysRevC.107.014326](https://doi.org/10.1103/PhysRevC.107.014326)

I. INTRODUCTION

Superheavy nuclei (SHN) with $Z \geq 104$ materialize because of the stabilizing shell correction energy. This shell correction energy creates a fission barrier that is nonexistent for these nuclei in the liquid-drop model because of the massive Coulomb repulsion between the protons. The notion of the stabilizing effects of shells points to the possible existence of a hypothetical island of stability inhabited by long-lived spherical superheavy nuclei. However, the predicted localizations of this island based on different theoretical approaches diverge. For instance, macroscopic-microscopic models (using Nilsson, Woods-Saxon, or folded-Yukawa potentials) predict the center to be around $Z = 114$, $N = 184$ [1,2] while the self-consistent models using Skyrme, Gogny, or relativistic mean field effective nuclear interactions predict stronger shell effects at $Z = 120, 124, 126$ and $N = 172, 184$ [3–6].

Therefore, a large body of experimental data of single and collective states gathered through prompt and decay spectroscopy is desirable to benchmark the theories that aim to describe the underlying nuclear structure in the superheavy mass region. The SHN are typically produced in fusion evaporation reactions with very low production cross sections (≈ 10 nb in the $A = 250$ region). The cross section diminishes even more as a function of atomic number [7]. As a result, the available spectroscopic data in the transfermium region are rather scarce [8]. Performing detailed spectroscopy in the

lighter transfermium region is thus more practical and one step closer to understanding the properties of the SHN. In this region, K isomers are of specific interest as they give information about the single-particle states near the Fermi level and their internal decay can populate states that are not normally accessible through α decay. In axially deformed nuclei, the K quantum number is the projection of the total angular momentum onto the symmetry axis. High- K isomerism occurs due to hindrance in electromagnetic transitions involving a large change in the K quantum number (from high K to low K for example). K isomers have been identified and/or suggested in several isotopes in this region (see Refs. [9–18]) and are also expected in ^{255}Rf . The ground-state configuration of ^{255}Rf is thought to be based on the $9/2^- [734]$ Nilsson orbital as in the lighter isotones (such a configuration has been unambiguously determined in ^{253}No through laser spectroscopy [19]).

In a recent study from GSI, two high- K isomers were observed with half-lives $T_{1/2} = 38_{-7}^{+12}$ μs and $T_{1/2} = 15_{-4}^{+6}$ μs , and were suggested to have spin $\geq 17/2 \hbar$ [20]. The excitation energies of these isomers were estimated to be 1.15–1.45 MeV and 0.9–1.2 MeV. In another study at GSI, an isomeric state with a half-life of $T_{1/2} = 50 \pm 17$ μs and an excitation energy of around 135 keV [21] was observed in α decay of ^{259}Sg to ^{255}Rf . The $5/2^+ [622]$ configuration was assigned to this isomer from the systematics in the lighter $N = 151$ isotones. Besides the $5/2^+ [622]$ spin isomer, two other excited states, $1/2^+ [620]$ around 510 keV and $11/2^- [725]$ around 600 keV, were also tentatively suggested in their work.

In this paper, we confirm the existence of two high- K isomers and the spin isomer in ^{255}Rf . We report on their half lives and excitation energies and suggest their most likely spins and parities. We also present a decay scenario, whose simulation

^{*} rikel.chakma@ganil.fr;

Present address: GANIL, 14000 Caen, France.

in GEANT4 [22] reproduces all of the spectroscopic observables and provides a measurement of the isomeric ratios.

II. EXPERIMENT

In this study, rutherfordium nuclei were produced in the fusion evaporation reaction of $^{207}\text{Pb}(^{50}\text{Ti}, 2n)^{255}\text{Rf}$ in two experimental campaigns at the FLNR facility of JINR in Dubna, Russia. The ^{50}Ti beam, having intensities $\approx 337\text{--}370$ pnA in the first campaign and $\approx 360\text{--}396$ pnA in the second and an average energy of ≈ 253 MeV in both, was delivered by the U400 cyclotron. The PbS targets [enriched with ^{207}Pb (96.2%), ^{208}Pb (2.6%), ^{206}Pb (1.1%), and ^{204}Pb (0.1%)] were $0.4\ \mu\text{g}/\text{cm}^2$ thick, deposited on $1.5\ \mu\text{m}$ Ti backings, and were mounted on a rotating target wheel. The evaporation residues (ERs) that emerged out of the target were separated using the velocity filter SHELS [23] and transported to the focal-plane detection setup, GABRIELA [24,25].

The ERs were implanted into a large-area double-sided silicon strip detector (DSSD) with the corresponding electronics [26] set to measure conversion electrons (up to 2 MeV) and α particles (up to 25 MeV) simultaneously. The fission fragments (typically > 60 MeV) thus were detected as overflows. The DSSD provided position and time correlations between the implanted ions and their successive decays. In the DSSD, isomeric decays were detected through Jones' calorimetric method [27] i.e., by measuring the low-energy signals (called CE henceforth) produced from the summation of total or partial energy depositions in the DSSD by internal conversion electrons (ICEs), x rays, and Auger and Coster-Kronig electrons. The calorimetric method is a powerful technique to evidence isomers whose decay proceeds by a cascade of highly converted transitions. In the case of short lifetimes and short cascades, however, the isomeric CE signals may be missed due to the dead time and thresholds of the electronics. In this study, the average threshold of the DSSD was between 60 and 100 keV, and the deadtime was $\approx 32\ \mu\text{s}$. To detect the ionizing particles (mostly ICEs) that escape the DSSD, a tunnel composed of eight small DSSDs is placed in the upstream direction of the large DSSD. Four coaxial, large volume germanium (Ge) detectors were mounted on each lateral side of the DSSD array and one clover detector [28] behind the DSSD to measure the x rays and γ rays. The average threshold of the tunnel detector was also between 60 and 100 keV and the energy resolution was $14.4(12)$ keV (full width at half maximum) at 320 keV. For the γ -ray detectors these corresponding values were ≈ 15 and $2.26(17)$ keV at 1332.5 keV.

III. RESULTS

A. Ground-state properties

In the two experimental campaigns, we produced a total of $\approx 7880(112)$ ^{255}Rf nuclei. Figure 1 shows a recoil-decay correlation plot, where the time between a decay event and an ER signal is plotted in \log_2 scale as a function of the decay energy. The half-life of the ground state of ^{255}Rf was measured from the time distribution of its characteristic α -decay events (in the 8660–8850 keV range) and fission events,

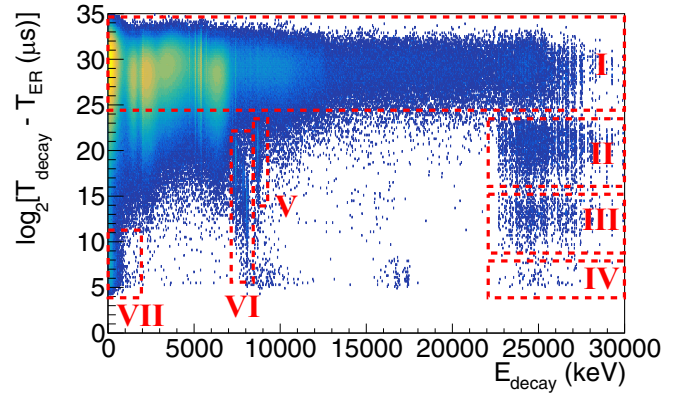


FIG. 1. Recoil-decay correlations measured in the DSSD for $^{207}\text{Pb}(^{50}\text{Ti}, xn)$. The relevant regions of the plot are marked I–VII and they correspond to random correlations (I), ^{255}Rf fission-decay events (II), ^{256}Rf fission-decay events (III), ^{254}Rf fission-decay events (IV), ^{255}Rf full-energy α -decay events (V), α -decay events of transfer products (VI), and CE signals from isomeric-decay events (VII).

and the values are $T_{1/2}^{\alpha} = 1.67 \pm 0.05$ s and $T_{1/2}^f = 1.69 \pm 0.03$ s respectively. The corresponding estimated branching ratios are $B_{\alpha} = 49.1 \pm 1.3\%$ and $B_f = 50.9 \pm 1.1\%$. These values are compatible with the reported values given in the literature [29–32]. Since no ^{255}Lr α decay was identified, an upper limit of the β^+/EC decay branch of ^{255}Rf was deduced as $B_{\text{EC}/\beta^+} = 0.06 \pm 0.02\%$.

B. Isomers

1. Detection of two isomeric transitions in cascade

After the detection of an ER and before the detection of the ground-state α or fission decay of ^{255}Rf , two CE signals in a cascade were detected in the DSSD. These decay chains are denoted as ER-CE-CE- ^{255}Rf , and a total of 27 such decay chains were detected. The energy and the time distributions of the first and second CEs are compared in Fig. 2, where one can notice that (a) the first isomer (iso1) is relatively longer lived than the second (iso2) and (b) the detected signal of iso1 is much smaller in energy than that of iso2. The lifetime of iso1 was measured with respect to the ER signals that precede them and that of iso2 with respect to iso1. Incidentally, no coincident γ rays or ICEs (in the tunnel detectors) were detected with the CE signals of iso1. However, six γ rays and eight ICEs were detected in coincidence with the CEs of iso2. The recorded energies of these γ rays are 166, 281, 470, 543, 551, and 778 keV and the electrons have energies below 160 keV. In the decay of iso2, by summing the energies of CEs with the energies of the coincident γ rays and electrons on an event-by-event basis, the total calorimetric energy (E_{calor}) was found to be ≈ 1 MeV. For iso1, E_{calor} is ≈ 200 keV as no coincident γ ray or ICEs were detected.

In some cases where only one CE signal in between an ER and the ground-state decay of ^{255}Rf was detected, it was still possible to assign two isomeric decays in a cascade using the germanium and tunnel detectors. γ rays and/or ICEs were

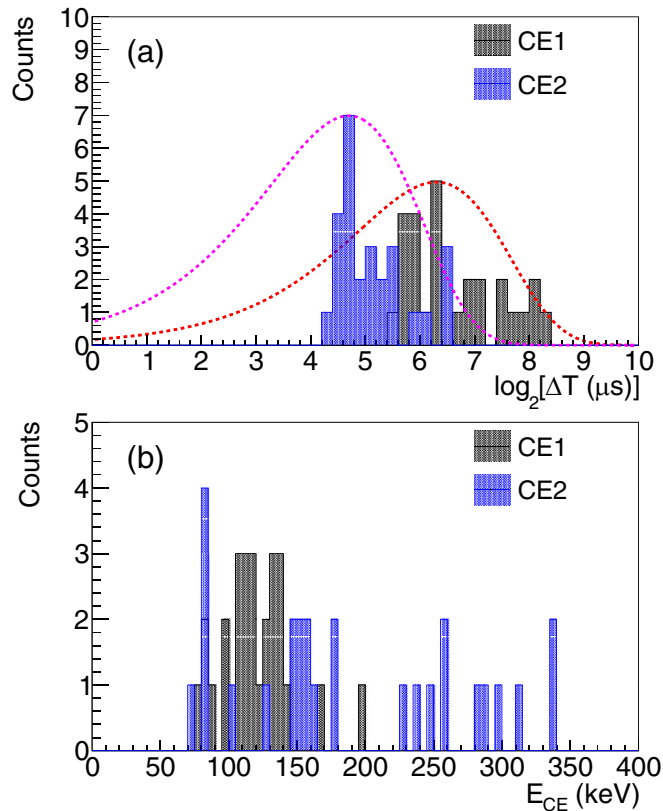


FIG. 2. (a) Time and (b) energy distribution comparisons between the CEs observed in the 27 ER-CE-CE- ^{255}Rf decay chains. The dotted lines in (a) are for guiding the eye.

detected in between the ER and CE signals, and, these decay chains are denoted as ER-[*]-CE- ^{255}Rf , where [*] = γ for γ rays and [*] = e^- for ICEs. We observed nineteen ER- γ -CE- ^{255}Rf and twenty-three ER- e^- -CE- ^{255}Rf correlations. In the ER- γ -CE- ^{255}Rf correlations, there were L x rays around 26 keV and a distinct 102 keV transition. No γ rays above 102 keV were observed, and the absence of K x rays in the γ -ray spectrum suggests that no transition in the decay from iso1 to iso2 lies above the K -shell binding energy (156.3 keV) of rutherfordium. In the electron spectrum, a peak around 80 keV, possibly from the L conversion of 102 keV transition and/or another transition with similar energy, was observed. From all these correlations, the half-lives of iso1 and iso2 were measured to be 49^{+13}_{-10} and 29^{+7}_{-5} μs respectively. Our data confirm the results of Ref. [20] that there are at least two isomers: iso1 and iso2; iso1 at excitation energy around 1.3 MeV and iso2 around 1 MeV above the ground state, and iso1 feeds iso2.

2. Detection of single isomeric transitions

A total of 701 CEs were detected between the ER implantation signals and ^{255}Rf ground-state decays. Out of these, 38 were preceded by γ rays or ICEs or both and were discussed in the previous section. The energy and time distribution (in \log_2 scale) of the remaining 663 CEs of the ER-CE- ^{255}Rf decay chains are shown in Fig. 3. The bulk of these CEs

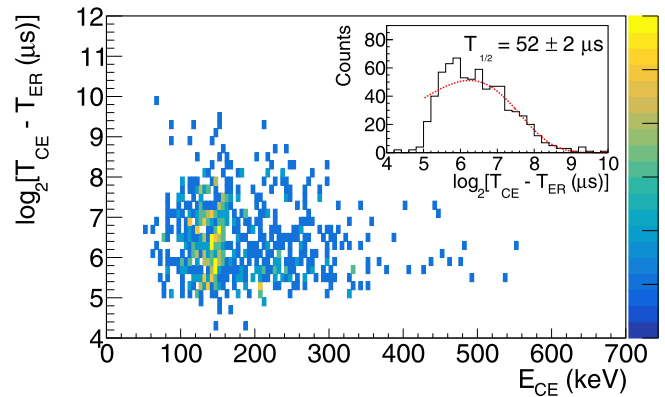


FIG. 3. Energy and time distribution plot of the CE signals observed in the decay chains ER-CE- ^{255}Rf . The inset shows the fit of the time distribution.

are concentrated around 145 keV, and their lifetimes seem slightly higher than those of the higher energy counterparts. The average half-life of these CEs is $T_{1/2} = 52 \pm 2$ μs .

In coincidence with the CEs in the decay chains of ER-CE- ^{255}Rf , 103 γ rays and 69 ICEs (in the tunnel detectors) were observed (see Fig. 4). In the γ -ray spectrum, the most intense lines are the 778 keV transition and L x rays around 24 keV. The 778, 543, and 170 keV transitions that are distinguishable in the γ -ray spectrum of ER-CE- ^{255}Rf were also seen in

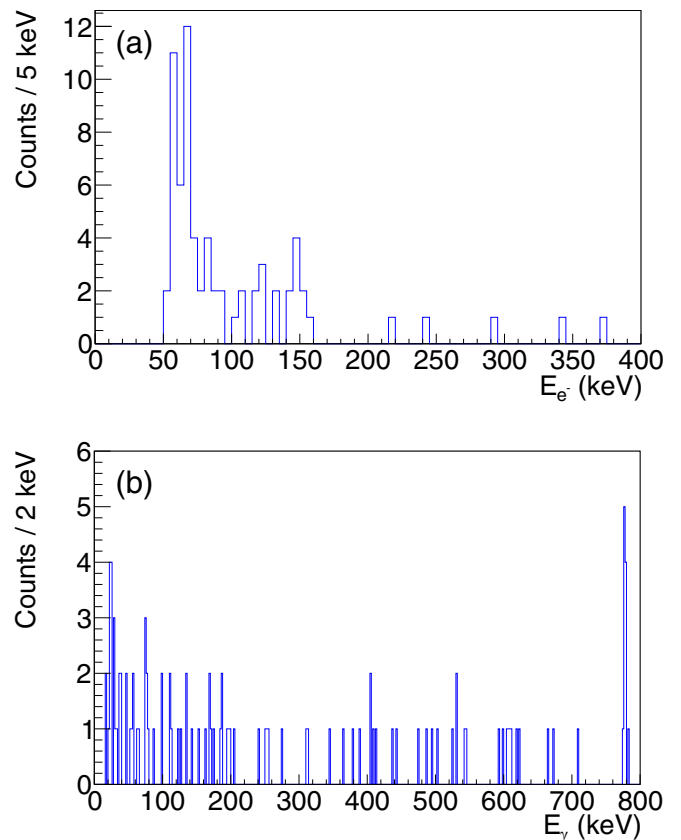


FIG. 4. Spectrum of (a) electrons in the tunnel detectors and (b) γ rays observed in coincidence with the CEs in the ER-CE- ^{255}Rf decay chains.

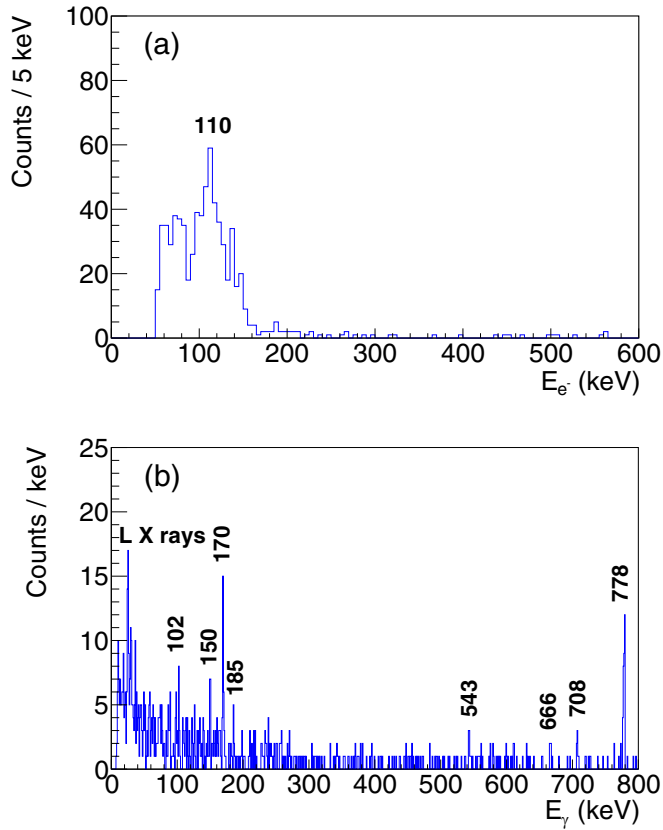


FIG. 5. Spectrum of (a) electrons in the tunnel detectors and (b) γ rays observed in the ER- γ/e^- - ^{255}Rf decay chains.

coincidence with iso2 in the ER-CE-CE- ^{255}Rf cascades (see the previous section). In the electron spectrum, two noticeable structures were observed: one below 100 keV and the other around ≈ 145 keV. Very few electrons were observed with energies between 200 and 400 keV. The measured E_{calor} involved in the deexcitation of the supposed isomer was found to be ≈ 1.1 MeV. This excitation energy corresponds to the one of iso2 in the two-CE-cascade correlations; however, the half-life is longer but is in line with the half-life of the $5/2^+$ spin isomer measured at GSI [21]. The spectrum of single isomeric decays is most likely complex, involving contributions from iso1, when iso2 goes undetected and vice versa, from iso2 alone and also from the $5/2^+$ spin isomer.

When no CEs are recorded in the implantation detector, thanks to the Ge and tunnel detectors again, single isomeric decays can still be detected in these detectors by looking at the γ rays and ICEs that follow an ER signal with a subsequent α or fission decay in the same pixel (ER- γ/e^- - ^{255}Rf). The E_{calor} obtained in this case from the summed energies of the coincident γ rays and electrons is ≈ 1 MeV, in agreement with the previous values. The energy spectra of these γ rays and electrons observed in this case are shown in Fig. 5. In the electron spectra, a peak around 110 keV is visible, but it is impossible to resolve other peaks and associate them to the observed γ -ray transitions.

In the γ -ray spectrum, we notice two prominent γ -ray lines: one at 778 keV and the other at 170 keV. Some weaker

TABLE I. Detector efficiency corrected intensities (I_γ) of the prominent γ -ray transitions following the decay of the isomeric states observed in this work. Intensities were normalized to the intensity of the 778 keV transition. The multipolarity of the 170 keV transition has been deduced from experiment while the counterparts for the other transitions are from the proposed decay scheme shown in Fig. 7. Spin assignments and branching ratios (b_γ) to these transitions are also from the proposed scheme (see Sec. IV for details).

E_γ (keV)	I_γ	b_γ (in %)	$I_i \rightarrow I_f$	Multipolarity
778	100(7)	59(5)	$(19/2^+) \rightarrow (17/2^-)$	$E1$
708	20(3)		$(17/2^-) \rightarrow (15/2^-)$	$M1$
666	16(2)	9(1)	$(19/2^+) \rightarrow (19/2^-)$	$E1$
610	13(2)		$(17/2^-) \rightarrow (17/2^-)$	$M1$
543	21(3)	12(2)	$(19/2^+) \rightarrow (21/2^-)$	$E1$
185	8(1)		$(17/2^-) \rightarrow (13/2^-)$	$E2$
170	34(4)	20(3)	$(19/2^+) \rightarrow (17/2^-)$	$E1$
150	15(2)	100	$(5/2^+) \rightarrow (9/2^-)$	$M2$
102	13(2)	100	$(21/2^+) \rightarrow (19/2^+)$	$M1$

transitions of energy 708, 666, 543, 185, 150, and 102 keV are also observable. Here one could argue that the 150 keV line is due to radiative process while filling vacancies of the K shell of rutherfordium. However, only ≈ 2 counts of $K_{\beta_1} = 150$ keV are expected from an estimation using the intensity of the K_{α_2} (126.3 keV) in contrast to 12 counts in the γ -ray spectrum, suggesting that the 150 keV line is indeed a real γ -ray transition.

The efficiency corrected intensities of the above transitions relative to the 778 keV line are given in Table I. From the γ -ray intensities, we can exclude the possibility of the 170 keV line being an $M1$ transition as we do not observe enough K x rays. If it were an $M1$ transition, we would expect to detect ≈ 106 counts at the energy of the Rf K_{α_2} energies, whereas only 8 counts were detected. Looking at the electron spectrum, we can also rule out the possibility of the 170 keV line being an $E2$ transition. If it were an $E2$ or an $M1$ transition, we would expect to detect ≈ 80 LMN+ ICEs with energies ranging 139–170 keV in the tunnel detector. But, in the electron spectrum, we have only a total of 110 counts in the 130–180 keV range, which includes the tail of the 110 keV main peak. If, on the other hand, the 170 keV line is an $E1$ transition, we would expect to detect only 1–2 counts.

To get a hint of the states involved in the 778, 666, 543, 170, and 98 keV (discussed later) transitions, their reduced hindrance factors f_ν were calculated. We calculated the f_ν values for $E1$, $M1$, and $E2$ electromagnetic multipolarities undergoing $\Delta K = 3, 4$, and 5 in each case. f_ν is defined as

$$f_\nu = F_W^{1/\nu}, \quad F_W = (T_{1/2}^\gamma / T_{1/2}^W) \quad (1)$$

where F_W is the hindrance of a given γ -ray transition, $T_{1/2}^\gamma$ is the partial γ -ray half-life determined experimentally, $T_{1/2}^W$ is the half-life calculated from Weisskopf single-particle estimates, and ν is the degree of K forbiddenness expressed as $\nu = \Delta K - L$ in which L is the multipolarity of the emitted radiation and ΔK is the change in K quantum number in

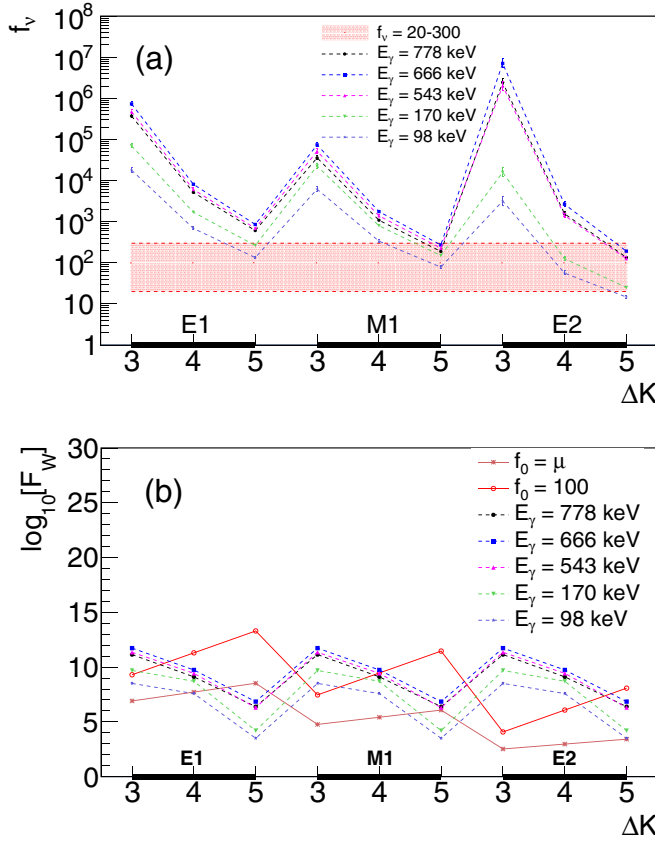


FIG. 6. (a) Measured f_v of the prominent γ -ray transitions observed in coincidence with the decay of iso1 and iso2, for $\Delta K = 3, 4$, and 5, having $E1, M1$, and $E2$ multiplicities in each case. The band gives the phenomenological range, $f_v = 20-300$, usually used to make spin-parity assignments. (b) Their corresponding F_W compared with the expected F_W after taking into account the multipolarity-dependent offset shown by $f_0 = \mu$ and $f_0 = 100$ line. The lines are there for guiding the eye.

transitioning from an initial state I_i to a final state I_f . Knowing the total internal conversion coefficient α_{Tot} of a γ -ray transition, its $T_{1/2}^\gamma$ can be calculated from the experimentally measured half-life $T_{1/2}^{\text{exp}}$ using the following relation:

$$T_{1/2}^\gamma = T_{1/2}^{\text{exp}} \times \frac{(1 + \alpha_{\text{Tot}})}{b_\gamma}. \quad (2)$$

$T_{1/2}^\gamma$ depends on the energy E_γ and the multipole order L of the emitted photon, the type of the transition σ (electric or magnetic) and on the nuclear structure entailed in the reduced transition probability $B(\sigma L, I_i \rightarrow I_f)$ [33]. Thus, F_W is a measure of the deviation of the true nuclear transition rate from the approximate single-particle model in which a single nucleon in an average potential deexcites the nucleus. Using the measured half-life of iso2, branching ratios given in Table I and internal conversion coefficients from BRICC [34], the f_v values for the 778, 666, 543, and 170 keV transitions were calculated. For the 98 keV transition, we used the half-life of iso1 and assumed 100% branching ratio in the decay of iso1 to iso2, as shown in Fig. 7. These measured f_v values

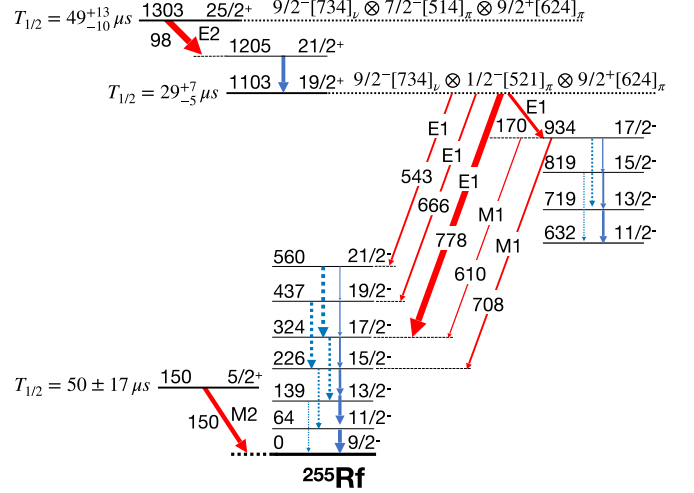


FIG. 7. Proposed partial level scheme for ^{255}Rf . The half-lives of the $19/2^+$ and $25/2^+$ are from this work, and that of the $5/2^-$ level is taken from Ref. [21].

are plotted in Fig. 6(a) in which the band shows the phenomenological range ($f_v = 20-300$) usually referred to for interpreting decay properties and assignment of spin-parity. In Fig. 6(a), it is indicative that the transitions emanating from iso2 can most likely involve $\Delta K = 5$. However, the types of these transitions cannot be determined. Figure 6(a) also suggests that they could be $M1$ or $E2$ transitions. But, on the other hand, it is also not uncommon to have large hindrances ($f_v \approx 1000$) for $E1$ transitions and it should also be emphasized that this phenomenological range is arbitrary, as the experimental data points on which it is based mainly in the works of Rusinov [35] and Löbner [36] are considerably scattered. Löbner pointed out that there is a dependence of hindrances on multiplicities. Kondev *et al.* with more experimental data later quantified these multipolarity-dependent offsets in their work [37] (see Table C of Ref. [37]). They have also shown that f_v is much smaller (represented here by $f_v = \mu$) compared to the commonly used Rusinov's empirical rule $f_v \approx 100$, i.e., the hindrance increases by a factor of approximately 100 with an increase of ΔK by 1 unit. We have compared the measured F_W with the expected values obtained after factoring in the multipolarity-dependent offsets on hindrances in Fig. 6(b). The figure shows two lines obtained using the relation $\log_{10} F_W = \log_{10} F_0 + \nu \log_{10} f_0$ [37]: (a) when $f_v = \mu$, using the fit parameters of Ref. [37], and (b) when $f_v = 100$ expected from Rusinov's empirical rule but with the same F_0 parameter of (a) to take into account the multipolarity dependency. Several trends can be noticed in Fig. 6(b): compared to (a), (b) overestimates the hindrances in all cases, (b) favors $\Delta K = 4$ $E1$ and $M1$ transitions and (a) favors $\Delta K = 5$ ($E1$) and ($M1$) transitions and $\Delta K = 4$ $E1$ transitions.

IV. DISCUSSIONS

To interpret the experimental results, we have relied heavily on GEANT4 simulations. The ground-state band of ^{255}Rf

TABLE II. Parameters used to build the rotational bands.

I^π	g_R	g_K	$\frac{\hbar^2}{2\mathcal{J}}$ (keV)	Q_0 (eb)
$9/2^-$	0.285	-0.25	5.8	12.42
$11/2^-$	0.285	-0.22	6.7	12.42
$19/2^+$	0.285	0.47	4.9	12.42

was built based on the ground-state band of the $N = 151$ neighboring isotone, i.e., ^{253}No [38]. The rotational g factor g_R was taken as $g_R = 0.7Z/A = 0.285$, where we have used a quenching factor of 0.7 to account for pairing effects [39]. The intrinsic quadrupole moment was taken as $Q_0 = 12.42$ eb using the predicted quadrupole deformation of $\beta_2 = 0.252$ [40]. We assumed these values remain constant for all other excited states. The single-particle g factors g_K in this work were obtained from deformed shell model calculations with a Woods Saxon potential using the prescription that the nucleon spin g factor is taken to be $0.7 \times g_{s\text{free}}$. For the $9/2^-$ [734] configuration, g_K was taken to be -0.25 . To build a rotational band, we also assumed a constant moment of inertia as follows:

$$E_K(I) = E_K(I_0) + \frac{\hbar^2}{2\mathcal{J}}[I(I+1) - K(K+1)], \quad (3)$$

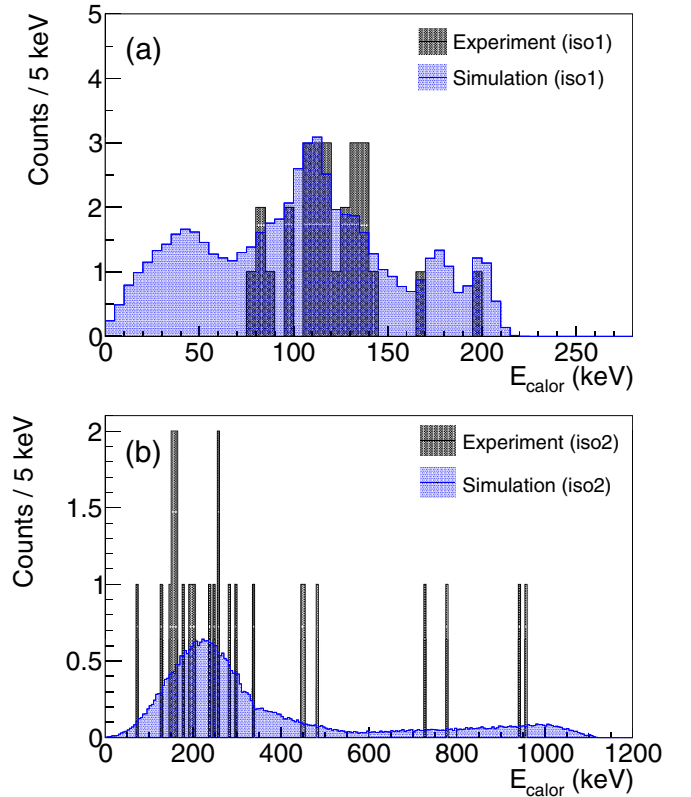
where $E_K(I_0)$ is the bandhead energy, I is the spin of the rotational state, and K is the total spin projection onto the symmetry axis. For the ground-state band, $\frac{\hbar^2}{2\mathcal{J}}$ was taken as 5.8 to have one in-band $E2$ transition around 185 keV, a peak observed experimentally at this energy. Similarly, for the $11/2^-$ [725] configuration, g_K was taken as -0.22 in accordance with the theoretical value $(g_K - g_R)/Q_0 = 0.040$ [18], and the rotational parameter was taken as $\frac{\hbar^2}{2\mathcal{J}} = 6.7$ to reproduce the rotational band observed in ^{257}Rf . The excitation energy of the $11/2^-$ state was taken to be around 600 keV as per the study of α decay of ^{259}Sg to ^{255}Rf [21]. We have adjusted the energies of the rotational states by a few keV to accommodate the observed γ -ray transitions. The $M1$ and $E2$ transition rates and the mixing ratios were computed using the standard formulas [33]. The conversion coefficients were obtained from BRICC [34], and for the intraband $M1/E2$ transitions, the conversion coefficients have been corrected using the relation

$$\alpha_{\text{mixed}}(M1, E2) = \frac{\alpha(M1) + \delta^2\alpha(E2)}{1 + \delta^2}, \quad (4)$$

where δ is the mixing ratio and is derived from the square root of the ratio of the transition rates $T_{i \rightarrow f}$:

$$\delta(E2/M1) = \sqrt{\frac{T_{i \rightarrow f}(E2)}{T_{i \rightarrow f}(M1)}}. \quad (5)$$

For the two observed isomers at excitation energies around ≈ 1.1 – 1.3 MeV, there are several possibilities: the odd neutron ($9/2^-$ [734]_v) can couple to the 5^- , 8^- , or 3^+ two-quasiproton states observed and/or suggested in ^{254}No and $^{254,256}\text{Rf}$. The 5^- and 8^- two-proton configurations are expected to be the lowest (see Table VII in Ref. [18]) and

FIG. 8. E_{calor} in the decay of (a) iso1 and (b) iso2.

lie close in energy. So, the possible high- K and low-lying one-neutron \otimes two-proton configurations for the isomers are therefore $\{9/2^- [734]_v \otimes 1/2^- [521]_\pi \otimes 9/2^+ [624]_\pi\}$ and $\{9/2^- [734]_v \otimes 7/2^- [514]_\pi \otimes 9/2^+ [624]_\pi\}$, yielding states with $K^\pi = 19/2^+$ and $25/2^+$.

Considering the constraints set by observables such as E_{calor} , $T_{1/2}$ and the intensities in the γ -ray, electron, and CE spectra, many decay scenarios were simulated and compared with the experimental results. The decay scenario shown in Fig. 7 is the final decay scheme whose simulation reproduced the experimental spectra very well.

In this scenario, the $19/2^+$ is placed at 1103 keV as per the E_{calor} of iso2. We assumed that the isomer decays to the ground state ($\Delta K = 5$) and to an intermediate structure $11/2^-$ [725] ($\Delta K = 4$) via $E1$ transitions. From intensity arguments (see Table I), the two most intense lines (778 and 170 keV transitions) must be parallel. We speculate that the 778 keV transition along with two other high energy lines (666 and 543 keV) populate the $17/2^-$, $19/2^-$, and $21/2^-$ states of the ground-state band. The 170 keV transition populates the $17/2^-$ state of the intermediate structure, which then decays to the ground-state band via two high energy $M1$ transitions. All $E1$ transitions have hindrances $f_v < 900$ (610_{-29}^{+42} , 857_{-47}^{+63} and 688_{-39}^{+52} for the 778, 666, and 543 keV transitions respectively) except for the 170 keV transition with $f_v = 1700_{-121}^{+164}$. These values are of the order of the values obtained for three $E1$ transitions deexciting the $21/2^+$ isomer in ^{257}Rf [18] and $\Delta K = 5$, 52 keV $E1$ transition from the 8^- isomer in ^{254}No [13].

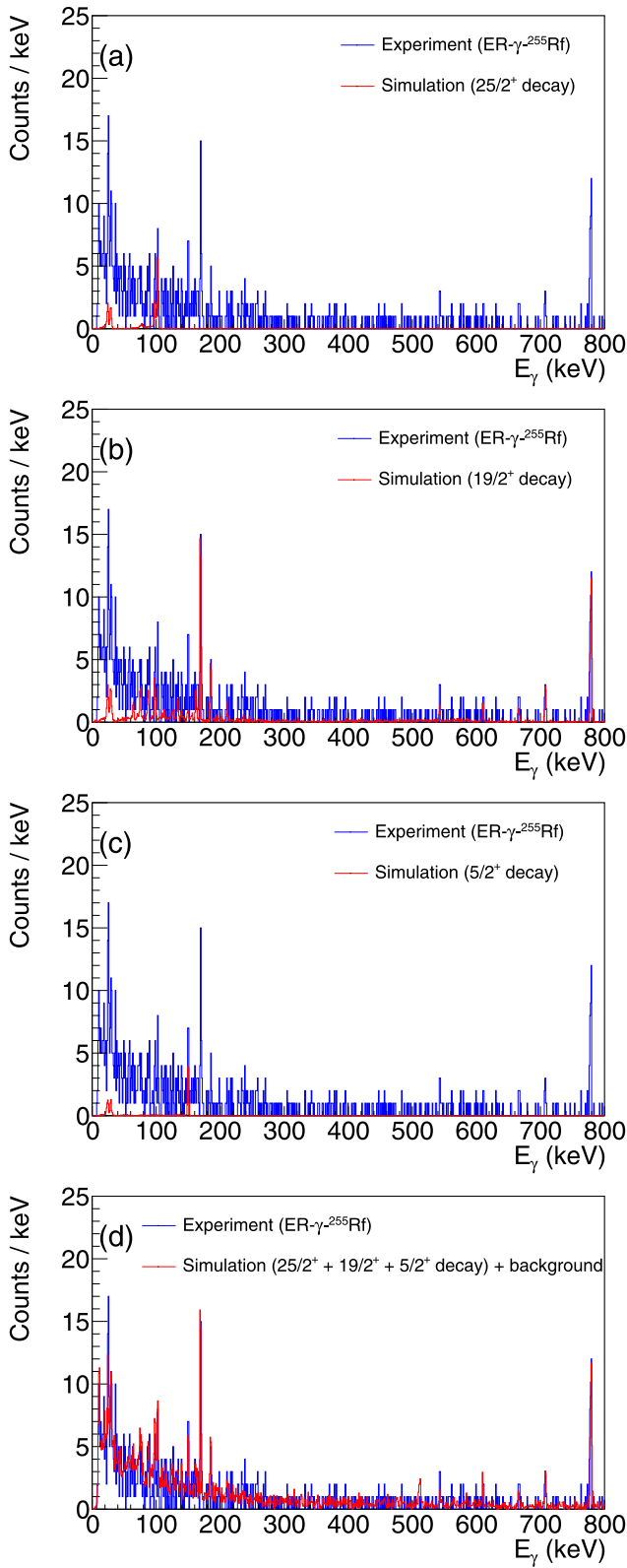


FIG. 9. Comparison of experimental γ -ray spectrum with simulations showing the contributions of (a) iso1, (b) iso2, (c) iso3 and (d) the total including normalized experimental background.

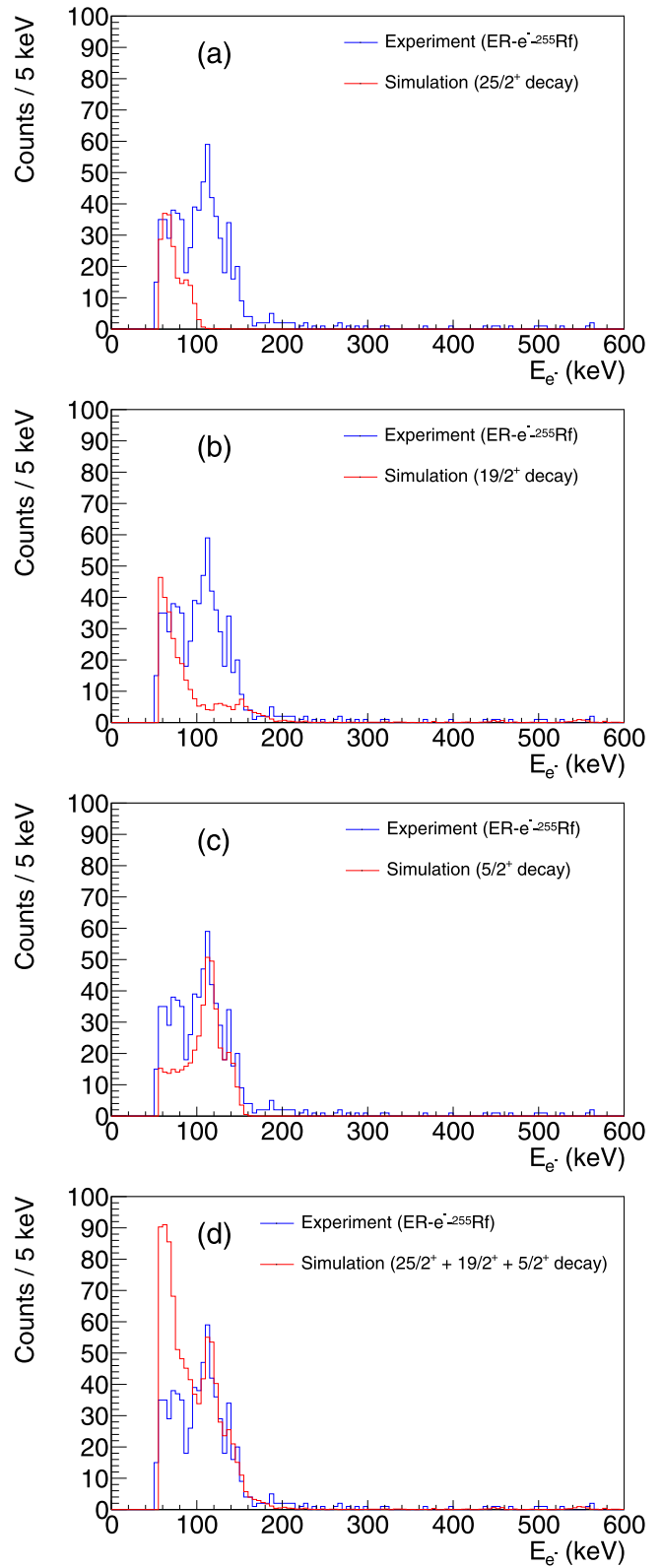


FIG. 10. Comparison of experimental electron spectrum with simulations showing the contributions of (a) iso1, (b) iso2, (c) iso3, and (d) the total.

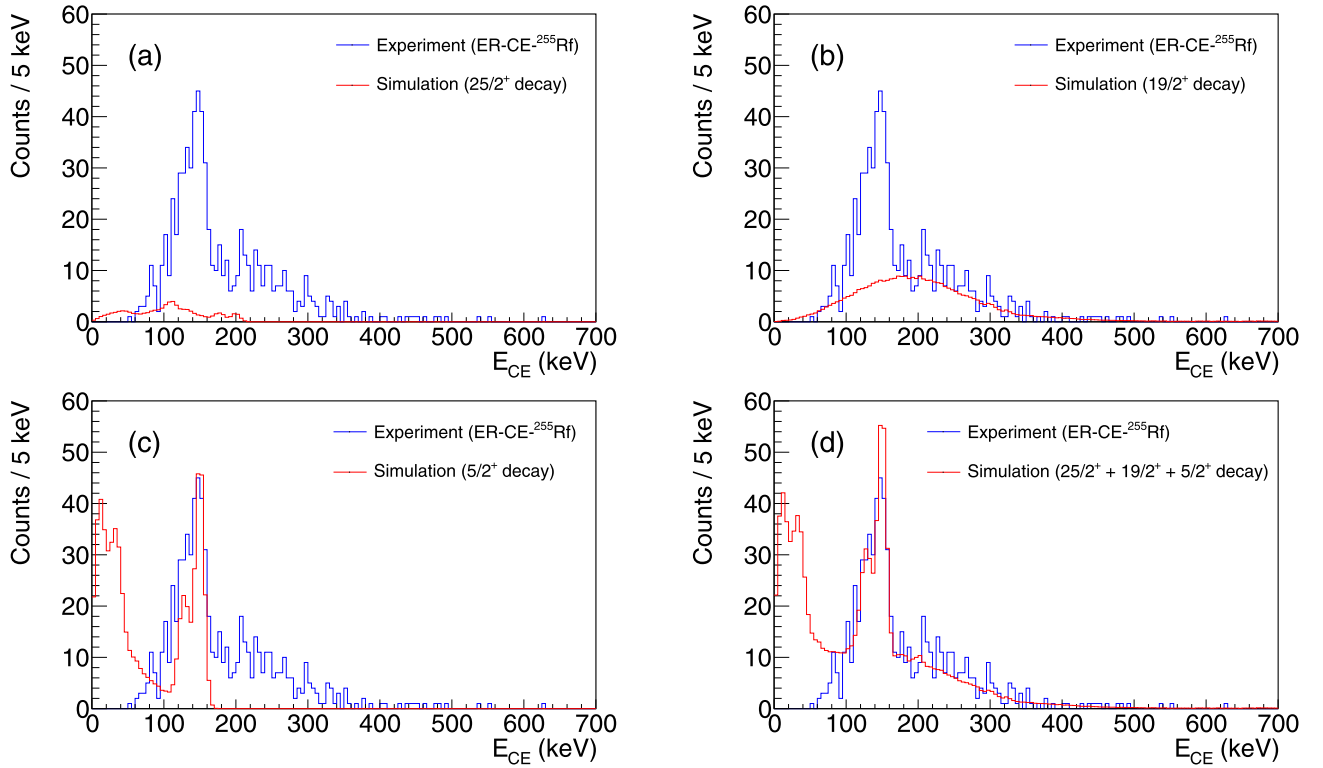


FIG. 11. Comparison of experimental CE spectrum with simulations showing the contributions of (a) iso1, (b) iso2, (c) iso3, and (d) the total.

Furthermore, the 708 and the 610 keV $M1$ transitions from the $17/2^-$ state of the $11/2^-$ band to the $17/2^-$ and the $15/2^-$ states of the ground state band seem to obey the Alaga intensity rule [41]. The expected branching ratio of these two transitions is $\langle \frac{17}{2} 1 \frac{11}{2} - 1 | \frac{17}{2} 1 \frac{17}{2} \frac{9}{2} \rangle / \langle \frac{17}{2} 1 \frac{11}{2} - 1 | \frac{17}{2} 1 \frac{15}{2} \frac{19}{2} \rangle = 0.76$ compared to $I_{610}/I_{708} = 0.65(12)$ experimentally. Note that, to fit the high energy lines, we have placed the $11/2^-$ band at 632 keV, which is slightly higher than what was inferred from α spectroscopy.

Regarding the $25/2^+$ isomer, $E_{\text{calor}} \leq 200$ sets a constraint on how far the $25/2^+$ isomer can be in energy from the $19/2^+$ isomer. It was assumed that a low energy $E2$ transition deexcites the $25/2^+$ (1303 keV) and populates the $21/2^+$ state of the $19/2^+$ band with a low energy $E2$ transition of 98 keV. Then an $M1$ transition of 102 keV to the $19/2^+$ state (observed experimentally) follows. To reproduce the 102 keV energy spacing, the rotational parameter $\frac{\hbar^2}{2\mathcal{I}}$ was taken as 4.9, which is acceptable for a band built on a three-quasiparticle configuration with reduced pairing. The parameters used to build the rotational bands are summarized in Table II. The $25/2^+$ isomer cannot be lower than the $21/2^+$, otherwise it would then have to decay to the $19/2^+$ band head via an $E3$ transition, and thus have a much longer lifetime. Assuming 100% branching ratio for the 98 keV transition from $K = 25/2$ to $K = 19/2$, a K hindrance of $f_v = 3183_{-650}^{+844}$ was obtained.

GEANT4 simulations of the decay of iso1 and iso2 reproduce quite well E_{calor} (see Fig. 8) and the γ -ray spectrum except for a deficit of L x rays. Deficits were also noticed in the simulated electron spectrum around 110 keV and in the CE

spectrum around 148 keV. These deficits were interpreted as the contribution of the $5/2^+$ [622] isomer (iso3) that decays to the ground state via an $M2$ transition, not included in the simulations thus far. The excitation energy which best fits the excess counts in the experimental spectra places the isomer at an excitation energy of 150 keV, just below the K -shell binding energy of rutherfordium. The significantly intense 150 keV line, whose nature was not understood *a priori* and is missing in the simulated spectrum, was also recovered. This excitation energy explains the lack of K x rays observed at GSI [21]. After adding the contribution of the $5/2^+$ isomer, the shape and intensity of the experimental CE and electron spectra are well reproduced. Figures 9, 10, and 11 show the contribution of each isomer in the γ -ray, electron, and CE spectra, respectively. Note that in Fig. 9(d), since there is no background in the simulations, a normalized experimental background has been added to the total simulated spectrum to compare with the experimental counterpart (see the Appendix). The iso1, given its low E_{calor} does not seem to contribute significantly to the electron and CE spectra. Despite this uncertainty of the excitation energy of iso1, simulations of the decay scheme reproduce the experimental spectra. The properties (spin and parity, excitation energy, and half-life) of these three isomers obtained in this work are compared with the values from literature in Table III.

For the simulations, we took the average threshold of the implantation detector to be 100 keV. After taking into account the threshold, the dead time associated with the implantation detector, and the lifetime of the isomers, we have estimated

TABLE III. Comparison of the properties (spin and parity I^π , excitation energy E^* , and half-life $T_{1/2}$) of the three isomers from this work with the values from literature.

This work			Literature			Ref.
I^π	E^* (MeV)	$T_{1/2}$ (μ s)	I^π	E^* (MeV)	$T_{1/2}$ (μ s)	
$25/2^+$	1.3	49^{+13}_{-10}		1.15–1.45	38^{+12}_{-7}	[20]
$19/2^+$	1.1	29^{+7}_{-5}	$>17/2$	0.9–1.2	15^{+6}_{-4}	[20]
$5/2^+$	0.150		$5/2^+$	≈ 0.135	50 ± 17	[21]

the number of the three isomers produced during the reaction (see Table IV). Although these suffer from uncertainties in the dead time and thresholds, they are consistent with known populations of low-lying one-particle and three-quasiparticle states. The difference in isomeric ratios of the two-high-K isomers may reflect the average spin populated in the reaction [42]. The goodness of the reproduction of all the experimental spectra gives confidence in the main features of the decay scheme shown in Fig. 7 and in the proposed configurations for the high- K isomers, which are in line with what is known in heavier rutherfordium isotopes. This decay scheme also suggests that the $11/2^-$ configuration may contain some vibrational component through mixing of the $11/2^-$ with the particle-phonon [$7/2^+[624] \otimes 2^-$]. Such a vibrational component has been predicted in the quasiparticle-phonon model [43].

V. CONCLUSION

From this study, we confirm the existence of three isomeric states in ^{255}Rf which are interpreted as the $5/2^+[622]_v$ spin isomer and two high- K^π $19/2^+$ and $25/2^+$ states interpreted as the coupling of $9/2^-[734]_v$ with $\{1/2^-[521]_\pi \otimes 9/2^+[624]_\pi\}_{5^-}$ and $\{7/2^-[514]_\pi \otimes 9/2^+[624]_\pi\}_{8^-}$ respectively. A tentative decay scheme has been proposed. GEANT4 simulations of this decay scheme were found to reproduce all the observables fairly well. Despite some uncertainties in the energy of the $E2$ transition of the $25/2^+$ isomer deexciting to the $19/2^+$ band (corresponding to a very large hindrance), the conclusions of this study should remain valid as it is constrained by the measured $E_{\text{calor}} \leq 200$ keV. The extracted isomeric ratios (which include dead-time and threshold effects) correspond to the ratios expected for one-particle and three-quasiparticle states in a reaction.

TABLE IV. Isomer populations and their isomeric ratios. To calculate these values, we varied the DSSD threshold from 60 to 100 keV in steps of 5 keV (bin width of the electron and CE spectra).

Isomer	I^π	Population	Isomeric ratio (%)
iso1	$25/2^+$	256^{+109}_{-79}	$3.3^{+1.4}_{-1.0}$
iso2	$19/2^+$	700^{+236}_{-197}	$8.9^{+3.0}_{-2.5}$
iso3	$5/2^+$	984 ± 170	12.5 ± 2.2

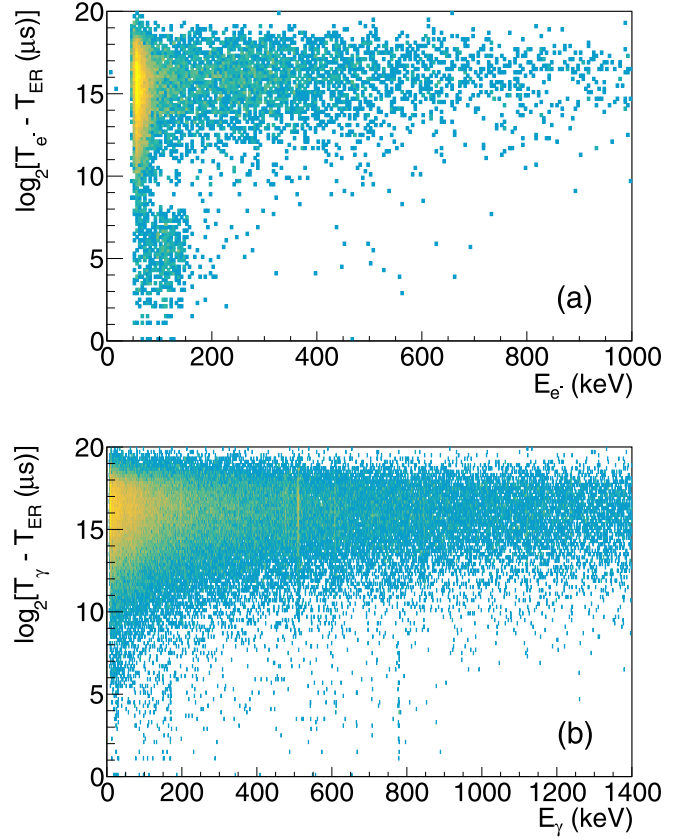


FIG. 12. Energy and time distributions of (a) electrons (in the tunnel detectors) and (b) γ rays detected after the detection of an ER but before the detection of ground state α or fission decay event of ^{255}Rf in the same DSSD pixel.

VI. OUTLOOK

The proposed decay scheme should be confirmed by repeating the experiment with better adapted electronics, perhaps with digital electronics coupled to faster and low-noise preamplifiers to lower the thresholds and the dead time. In particular, the prompt high energy transitions could be ascertained by performing prompt spectroscopy at the target for ^{255}Rf as in the case of ^{253}No . This could be attempted using JUROGAM spectrometer at RITU in Jyväskylä. However, as the cross section is low and the flux is fragmented, such an experiment will probably require a next-generation γ -ray spectrometer such as AGATA [44]. One could also repeat the experiment on the α decay of ^{259}Sg to ^{255}Rf to measure the decay properties of $11/2^-$ and $5/2^+$ states similar to what was done in the case of ^{257}Rf to ^{253}No [45].

ACKNOWLEDGMENTS

This work was supported by the Russian Foundation for Basic Research (Project No. 18-52-15004), the French National Research Agency (Projects No. ANR-06-BLAN-0034-01 and No. ANR-12-BS05-0013), and the IN2P3-JINR Collaboration Agreement No. 04-63.

APPENDIX: SOURCES OF BACKGROUND IN THE EXPERIMENTAL SPECTRA

The random correlations in the DSSD (Fig. 1), tunnel [Fig. 12(a)], and Ge [Fig. 12(b)] detectors mainly occur from the decay of beam- and/or target-like transfer products, long-lived nuclei produced in the calibration reactions or during previous irradiation. In the γ -ray spectrum, there are also contributions from terrestrial sources such as ^{40}K (1460 keV), ^{214}Bi (610 and 1120 keV), ^{228}Ac (912 and 966 keV), ^{208}Tl (584 keV), ^{212}Pb (238 keV), ^{232}Th , ^{238}U , and electron and positron annihilation radiation (511 keV). To exclude the

random correlations from the γ -ray and electron spectra the search time was limited to $\log_2 \Delta T = 8.6 = 388 \mu\text{s}$, the lifetime limit seen in Fig. 2(a). This gate removes the random correlations in the electron spectrum but not completely in the γ -ray spectrum, especially on the lower energy side. To compare the simulated γ -ray spectrum with the experimental one in Fig. 9(d), the events in the time window from $\log_2 \Delta T = 9 = 512 \mu\text{s}$ to $\log_2 \Delta T = 12 = 4096 \mu\text{s}$ in the energy-time matrix shown in Fig. 12(b) were taken as the background. This projected energy spectrum was then normalized to the experimental one where no peaks are observed.

- [1] S. G. Nilsson, C. F. Tsang, A. Sobczewski, Z. Szymański, S. Wycech, C. Gustafson, I. Lamm, P. Möller, and B. Nilsson, *Nucl. Phys. A* **131**, 1 (1969).
- [2] R. R. Chasman, I. Ahmad, A. M. Friedman, and J. R. Erskine, *Rev. Mod. Phys.* **49**, 833 (1977).
- [3] S. Ćwiok, J. Dobaczewski, P.-H. Heenen, P. Magierski, and W. Nazarewicz, *Nucl. Phys. A* **611**, 211 (1996).
- [4] K. Rutz, M. Bender, T. Bürvenich, T. Schilling, P.-G. Reinhard, J. A. Maruhn, and W. Greiner, *Phys. Rev. C* **56**, 238 (1997).
- [5] M. Bender, K. Rutz, P.-G. Reinhard, J. A. Maruhn, and W. Greiner, *Phys. Rev. C* **60**, 034304 (1999).
- [6] A. T. Kruppa, M. Bender, W. Nazarewicz, P.-G. Reinhard, T. Vertse, and S. Ćwiok, *Phys. Rev. C* **61**, 034313 (2000).
- [7] S. Hofmann, S. N. Dmitriev, C. Fahlander, J. M. Gates, J. B. Roberto, and H. Sakai, *Pure. Appl. Chem.* **90**, 1773 (2018).
- [8] C. Theisen, P. T. Greenlees, T.-L. Khoo, P. Chowdhury, and T. Ishii, *Nucl. Phys. A* **944**, 333 (2015).
- [9] B. Sulignano, S. Heinz, F. P. Heßberger, S. Hofmann, D. Ackermann, S. Antalic *et al.*, *Eur. Phys. J. A* **33**, 327 (2007).
- [10] A. Lopez-Martens, T. Wiborg-Hagen, K. Hauschild, M. L. Chelnokov, V. I. Chepigin, D. Curien *et al.*, *Nucl. Phys. A* **852**, 15 (2011).
- [11] S. K. Tandel, T. L. Khoo, D. Seweryniak, G. Mukherjee, I. Ahmad, B. Back *et al.*, *Phys. Rev. Lett.* **97**, 082502 (2006).
- [12] R.-D. Herzberg, P. T. Greenlees, P. A. Butler, G. D. Jones, M. Venhart, I. G. Darby *et al.*, *Nature (London)* **442**, 896 (2006).
- [13] R. M. Clark, K. E. Gregorich, J. S. Berryman, M. N. Ali, J. M. Allmond, C. W. Beausang *et al.*, *Phys. Lett. B* **690**, 19 (2010).
- [14] K. Hauschild, A. Lopez-Martens, A. V. Yeremin, O. Dorvaux, S. Antalic, A. V. Belozеров *et al.*, *Phys. Rev. C* **78**, 021302(R) (2008).
- [15] H. M. David, J. Chen, D. Seweryniak, F. G. Kondev, J. M. Gates, K. E. Gregorich *et al.*, *Phys. Rev. Lett.* **115**, 132502 (2015).
- [16] A. P. Robinson, T. L. Khoo, D. Seweryniak, I. Ahmad, M. Asai, B. B. Back *et al.*, *Phys. Rev. C* **83**, 064311 (2011).
- [17] H. B. Jeppesen, I. Dragojević, R. M. Clark, K. E. Gregorich, M. N. Ali, J. M. Allmond *et al.*, *Phys. Rev. C* **79**, 031303(R) (2009).
- [18] J. Rissanen, R. M. Clark, K. E. Gregorich, J. M. Gates, C. M. Campbell, H. L. Crawford *et al.*, *Phys. Rev. C* **88**, 044313 (2013).
- [19] S. Raeder, D. Ackermann, H. Backe, R. Beerwerth, J. C. Berengut, M. Block *et al.*, *Phys. Rev. Lett.* **120**, 232503 (2018).
- [20] P. Mosat, F. P. Heßberger, S. Antalic, D. Ackermann, B. Andel, M. Block, S. Hofmann, Z. Kalaninova, B. Kindler, M. Laatiaoui, B. Lommel, A. K. Mistry, J. Piot, and M. Vostinar, *Phys. Rev. C* **101**, 034310 (2020).
- [21] S. Antalic, F. P. Heßberger, D. Ackermann, S. Heinz, S. Hofmann, B. Kindler, J. Khuyagbaatar, B. Lommel, and R. Mann, *Eur. Phys. J. A* **51**, 41 (2015).
- [22] S. Agostinelli, J. Allison, K. Amako, J. Apostolakis, H. Araujo, P. Arce *et al.*, *Nucl. Instrum. Methods A* **506**, 250 (2003).
- [23] A. G. Popeko, A. V. Yeremin, O. N. Malyshev, V. I. Chepigin, A. V. Isaev, Yu. A. Popov, A. I. Svirikhin, K. Hauschild, A. Lopez-Martens, K. Rezyunkina, and O. Dorvaux, *Nucl. Instrum. Methods B* **376**, 140 (2016).
- [24] R. Chakma, K. Hauschild, A. Lopez-Martens, A. V. Yeremin, O. N. Malyshev, A. G. Popeko, Yu. A. Popov, A. I. Svirikhin, V. I. Chepigin, O. Dorvaux, B. Gall, and K. Kessaci, *Eur. Phys. J. A* **56**, 245 (2020).
- [25] K. Hauschild, A. V. Yeremin, O. Dorvaux, A. Lopez-Martens, A. V. Belozеров, C. Briançon *et al.*, *Nucl. Instrum. Methods A* **560**, 388 (2006).
- [26] A. V. Isaev, A. V. Yeremin, N. I. Zamyatin, A. N. Kuznetsov, O. N. Malyshev, A. I. Svirikhin, M. L. Chelnokov, V. I. Chepigin, K. Hauschild, A. Lopez-Martens, and O. Dorvaux, *Instrum. Exp. Tech.* **54**, 37 (2011).
- [27] G. Jones, *Nucl. Instrum. Methods A* **488**, 471 (2002).
- [28] G. Duchêne, F. A. Beck, P. J. Twin, G. de France, D. Curien, L. Han, C. W. Beausang, M. A. Bentley, P. J. Nolan, and J. Simpson, *Nucl. Instrum. Methods A* **432**, 90 (1999).
- [29] F. P. Heßberger, G. Münzenberg, S. Hofmann, W. Reisdorf, K. H. Schmidt, H. J. Schött, P. Armbruster, R. Hingmann, B. Thuma, and D. Vermeulen, *Z. Phys. A* **321**, 317 (1985).
- [30] F. P. Heßberger, S. Hofmann, V. Ninov, P. Armbruster, H. Folger, G. Münzenberg, H. J. Schött, A. G. Popeko, A. V. Yeremin, A. N. Andreyev, and S. Saro, *Z. Phys. A* **359**, 415 (1997).
- [31] F. P. Heßberger, S. Hofmann, D. Ackermann, V. Ninov, M. Leino, G. Münzenberg, S. Saro, A. Lavrentev, A. G. Popeko, A. V. Yeremin, and C. Stodel, *Eur. Phys. J. A* **12**, 57 (2001).
- [32] F. P. Heßberger, S. Hofmann, D. Ackermann, S. Antalic, B. Kindler, I. Kojouharov, P. Kuusiniemi, M. Leino, B. Lommel, R. Mann, K. Nishio, A. G. Popeko, B. Sulignano, S. Saro, B. Streicher, M. Venhart, and A. V. Yeremin, *Eur. Phys. J. A* **30**, 561 (2006).
- [33] P. Ring and P. Schuck, *The Nuclear Many-Body Problem* (Springer-Verlag, Berlin, 1980).

- [34] T. Kibédi, T. W. Burrows, M. B. Trzhaskovskaya, P. M. Davidson, and C. W. Nestor Jr., *Nucl. Instrum. Methods A* **589**, 202 (2008).
- [35] L. I. Rusinov, *Usp. Fiz. Nauk* **73**, 615 (1961).
- [36] K. E. G. Löbner, *Phys. Lett. B* **26**, 369 (1968).
- [37] F. G. Kondev, G. D. Dracoulis, and T. Kibédi, *At. Data Nucl. Data Tables* **105-106**, 105 (2015).
- [38] A. K. Mistry, R.-D. Herzberg, P. T. Greenlees, P. Papadakis, K. Auranen, P. A. Butler *et al.*, *Eur. Phys. J. A* **53**, 24 (2017).
- [39] N. J. Stone, J. R. Stone, P. M. Walker, and C. R. Bingham, *Phys. Lett. B* **726**, 675 (2013).
- [40] P. Möller, A. J. Sierk, T. Ichikawa, and H. Sagawa, *At. Data Nucl. Data Tables* **109-110**, 1 (2016).
- [41] G. Alaga, K. Alder, A. Bohr, and B. R. Mottelson, *Dan. Mat. Fys. Medd.* **29**(9), 1 (1955).
- [42] G. Henning, T. L. Khoo, A. Lopez-Martens, D. Seweryniak, M. Alcorta, M. Asai *et al.*, *Phys. Rev. Lett.* **113**, 262505 (2014).
- [43] N. Yu. Shirikova, A. V. Sushkov, L. A. Malov, and R. V. Jolos, *Eur. Phys. J. A* **51**, 21 (2015).
- [44] S. Akkoyun, A. Algora, B. Alikhani, F. Ameil, G. de Angelis, L. Arnold *et al.*, *Nucl. Instrum. Methods A* **668**, 26 (2012).
- [45] K. Hauschild, A. Lopez-Martens, R. Chakma, M. L. Chelnokov, V. I. Chepigin, A. V. Isaev *et al.*, *Eur. Phys. J. A* **58**, 6 (2022).

Correction: The previously published Figure 7 contained an error in the excitation energy of the $25/2^+$ state and has been replaced. Corresponding changes have been made in the last sentence of Sec. III B 1, first sentence of second paragraph of Sec. IV, second sentence of sixth paragraph of Sec. IV, and second column of Table III.